IMAGE EUV observation of radially bifurcated plasmaspheric features: First observations of a possible standing ULF waveform in the inner magnetosphere

M. L. Adrian

Center for Space Plasma and Aeronomic Research, University of Alabama in Huntsville, Huntsville, Alabama, USA

D. L. Gallagher and L. A. Avanov

Science Directorate, NASA Marshall Space Flight Center, Huntsville, Alabama, USA

Received 4 April 2003; revised 29 August 2003; accepted 10 September 2003; published 6 January 2004.

[1] We present EUV observations of the plasmasphere from 1938 to 2211 UT on 28 June 2000 characterized by the presence of bifurcated radial enhancements of the He^+ plasma distribution in the nightside sector. These features remain stable throughout the period of observation and are found to move about the Earth at 67% of the corotation rate. Two-dimensional simulation of the plasmasphere assuming the presence of an azimuthal standing wave patterns at L = 1.8 and 2.5 suggests that the organization of the outer plasmasphere is the result of convective motion driven by a ULF standing wave. Preliminary analysis of ground-based magnetometer data provided by the IMAGE magnetometer network during the period of EUV observation indicates the presence of several narrow-frequency oscillations extending down to 0.68 mHz, consistent with simulation results. Similar narrow-frequency features are found in preliminary analysis of ACE Solar Wind Electron Proton Alpha Monitor (SWEPAM) bulk solar wind velocity data. We speculate that the observed radial He^+ enhancements of the nightside plasmasphere may be the result of a nonresonant oscillation driven by the solar wind. *INDEX TERMS:* 2768 Magnetospheric Physics: Plasmasphere; 2730 Magnetospheric Physics: Magnetosphere—inner; 2760 Magnetospheric Physics: Plasma convection; 2752 Magnetospheric Physics: MHD waves and instabilities; *KEYWORDS:* plasmasphere, inner magnetosphere, magnetospheric configuration and dynamics, MHD waves and instabilities, solar wind/magnetosphere interactions

Citation: Adrian, M. L., D. L. Gallagher, and L. A. Avanov (2004), IMAGE EUV observation of radially bifurcated plasmaspheric features: First observations of a possible standing ULF waveform in the inner magnetosphere, *J. Geophys. Res.*, *109*, A01203, doi:10.1029/2003JA009974.

1. Introduction

[2] The plasmasphere is a torus of cold (electron temperature $T_e \sim 1$eV), dense (electron density $N_e \sim 10^2 - 10^4$ cm^{-3}) plasma that encircles the Earth. In a quasi-stationary view of plasmaspheric dynamics [*Nishida*, 1966; *Brice*, 1967], the cold dense plasma near Earth at low latitudes occupies magnetic flux tubes that follow drift trajectories that corotate with the Earth and are filled by ionospheric outflows over periods ranging from several hours to days. Outside of a boundary called the ''last closed equipotential'' or the ''separatrix,'' flux tubes drift under the influence of the globally sunward magnetospheric convection and receive limited filling from ionospheric sources. Consequently, flux tubes outside the separatrix have much lower densities ($10^{-1} - 10^1$ cm^{-3}) than those inside. In this quasi-stationary view, the separatrix that divides the corotating, high-density plasma of the plasmasphere from the convection-driven, low-density plasma of the inner magnetosphere coincides with the plasmapause.

0148-0227/04/2003JA009974$09.00

[3] The plasmapause, generally identified as the sharp density gradient between the $10^2 - 10^4$ cm^{-3} plasmaspheric plasmas and the $10^{-1} - 10^1$ cm^{-3} plasmas of the magnetospheric trough, was first discovered in both the ground-based whistler measurements of *Carpenter* [1963] and satellite in situ plasma measurements of *Gringauz* [1963]. At times, a plasmapause or sharp gradient in plasmaspheric density is not present. Instead densities, particularly during quite times, gradually decrease with increasing distance from the Earth. When the plasmapause is present, it is characterized by a one to two orders of magnitude decrease in density over a radial distance as little as 0.1 R_E. Additionally, the outer plasmasphere and plasmapause region can display variable structure such as a featureless steep gradient, featureless with ramp, featureless with an outer radial enhancement, multiple plateaus, featureless plasmapause with trough, multiple plateaus with trough, and other complex structures [*Horwitz et al.*, 1990]. Since the plasmasphere responds to erosion and refilling over a wide range of timescales and is subject to the spatially structured and unsteady nature of magnetospheric convection, the portrayal of the plasmapause as a mere separatrix

between corotation and convective flows is an oversimplification at best.

[4] The outer plasmasphere, plasmapause and magnetospheric trough are also regions permeated by extensive hydromagnetic wave activity. Numerous studies have found ULF magnetohydrodynamic waves with quasi-monochromatic wave trains driven by broad band sources like Kelvin-Helmholtz instabilities, solar wind pressure pulses, and flux transfer events [*Samson et al.*, 1992]. The monochromatic character of these wave trains suggests their generation by MHD cavities [*Kivelson and Southwood*, 1985]. Increasingly, these studies have observed that field line resonances exist only at persistent discrete frequencies [*Samson et al.*, 1992; *Lessard et al.*, 2003]. In addition, numerical simulations suggest the presence of a magnetospheric "shoal" in the evening sector of the outer plasmasphere upon which MHD waves break [*Moore et al.*, 1987]. The presence of MHD cavity mode field line resonances may also serve to complicate the detection and/or identification of the plasmapause by introducing greater structure to the interface between plasmaspheric and trough plasmas.

[5] With launch of the Imager for Magnetopause-to-Aurora Global Exploration (IMAGE) satellite carrying the Extreme Ultraviolet Imager (EUV) on 25 March 2000, the structure of the plasmasphere and plasmapause are monitored in near real time. We present observations of the plasmasphere on 28 June 2000 that are characterized by bifurcated radial enhancements in the He^+ distribution in the nightside sector. This observed "pattern" in the outer plasmasphere is found to lag with respect to corotation with the Earth and suggests the "organization" of plasma dictated by the presence of a ULF standing wave pattern. The plasmaspheric observations on 28 June 2000 represent the most striking example to date of a class of plasmaspheric structures that offer new insight into the dynamics of the inner magnetosphere.

2. Instrumentation

[6] With an average number density of $\sim 10^3$ cm^{-3} at $L \approx 3$, H^+ is the dominant plasmaspheric ion species, comprising $\sim$80% of the total number density. Unfortunately, H^+ has no optical emission to be exploited for remote sensing of the plasmasphere. However, significant concentrations of He^+ (typically $He^+/H^+ \sim 0.1-0.2$) and O^+ (typically $O^+/H^+ \sim 0.05-0.10$) exist in the plasmasphere [*Craven et al.*, 1997; *Comfort et al.*, 1988], with both species offering the potential for remote sensing of the plasmasphere through resonance scattering of extreme ultraviolet (EUV) emission. The feasibility of remote sensing of He^+ resonantly scattered 30.4 nm EUV has been demonstrated [*Weller and Meier*, 1974; *Meier and Weller*, 1974; *Chakrabarti et al.*, 1982; *Swift et al.*, 1989] through the imaging of limited portions of the plasmasphere [*Meier et al.*, 1998; *Nakamura et al.*, 2000].

[7] As described by *Sandel et al.* [2000, 2001] the IMAGE Extreme Ultraviolet Imager (EUV) consists of three wide-field (30°) cameras tuned to detect the 30.4-nm resonance line of plasmaspheric He^+. The field of view (FOV) of the three cameras overlaps slightly to form a fan-shaped instantaneous FOV of dimensions 84° × 30°. As the IMAGE satellite proceeds through a single spin, the fan-shaped FOV of EUV sweeps across an 84° × 360° swath of sky recording the intensity of detected 30.4-nm radiation in an array of about 0.6° × 0.6° pixels. Since the plasmaspheric He^+ scattered 30.4-nm emission is an optically thin medium, the measured intensity is directly proportional to the He^+ column density along the line of sight through the plasmasphere. Each frame of EUV data presented below is produced from a 10-min accumulation that encompasses five spins of the IMAGE satellite.

3. Observation

[8] We present IMAGE EUV data acquired on 28 June 2000 (day 180) principally between 1930 and 2200 UT. Figure 1 presents the IMAGE orbit for day 180 from 1200 to 2300 UT in Solar Magnetic (SM) coordinates. During this period of EUV observations (highlighted in gray) the IMAGE satellite orbit was roughly constrained to the dawn-dusk plane with the satellite passing nearly over the northern magnetic pole from dusk toward dawn. As a result, most of the EUV observations of the plasmasphere were recorded directly over the north magnetic pole or, during the later period of observation, with the instrument looking back toward the dusk region. As presented in Figure 2, these observations take place during a period of relatively quite geomagnetic conditions. A weak geomagnetic storm parameterized by $Dst \approx -75$ nT, $Kp \approx 6$, and $Ap \approx 80$ occurred at $\sim$1700 UT on 26 June 2000 (day 178), after which time, conditions quieted. During the period of EUV observations, an even weaker disturbance of $Dst \approx -37$ nT accompanied by $Kp \approx 3$, and $Ap \approx 20$ had just commenced.

3.1. Feature Identification

[9] Figure 3 presents an example of EUV data recorded between 1930 and 2200 UT on 28 June 2000. Figure 3a shows the EUV image taken at 2029 UT that is logarithmically scaled as a function of counts. The location of Earth is shown as a circle with the white cross indicating Earth's center. For reference and perspective, dipole field lines for $L = 2$ and 3 have been overlaid on the image at 0600, 1200, 1800, and 2400 MLT. The field lines at 1200 MLT are shown in yellow and are supplemented by a yellow arrow and annotation that indicate the direction to the Sun. A weak signature of Earth's shadow is seen opposite the Sun direction. As with many EUV images recorded to date, the auroral oval is visible due to leakage of an ionospheric O^+ 53.9-nm line through the instrument band-pass filter [*Burch et al.*, 2001]. In addition, band-pass filter leakage of the ionospheric O^+ 53.9-nm line, a neutral ionospheric helium line at 58.4 nm, and an ionospheric He^+ line at 30.4 nm contribute to produce the enhanced arc of airglow intensity along the dayside limb of the Earth [*Sandel et al.*, 2003]. Immediately apparent in the image is the lack of a sharp, distinct "He^+ edge" [*Goldstein et al.*, 2003] typically used to identify the location of the plasmapause. Figure 3a represents a (somewhat) typical view of the plasmasphere under quite geomagnetic conditions as seen by EUV. Despite its seemingly "diffuse" nature, the plasmapause occurs at $L \sim 3$. Closer examination of the nightside plasmasphere and plasmapause indicates the presence of several radial enhancements in the He^+ distribution. Additionally, at $L \sim 1.8$ the radial enhancements at $\sim$2300, 0000,

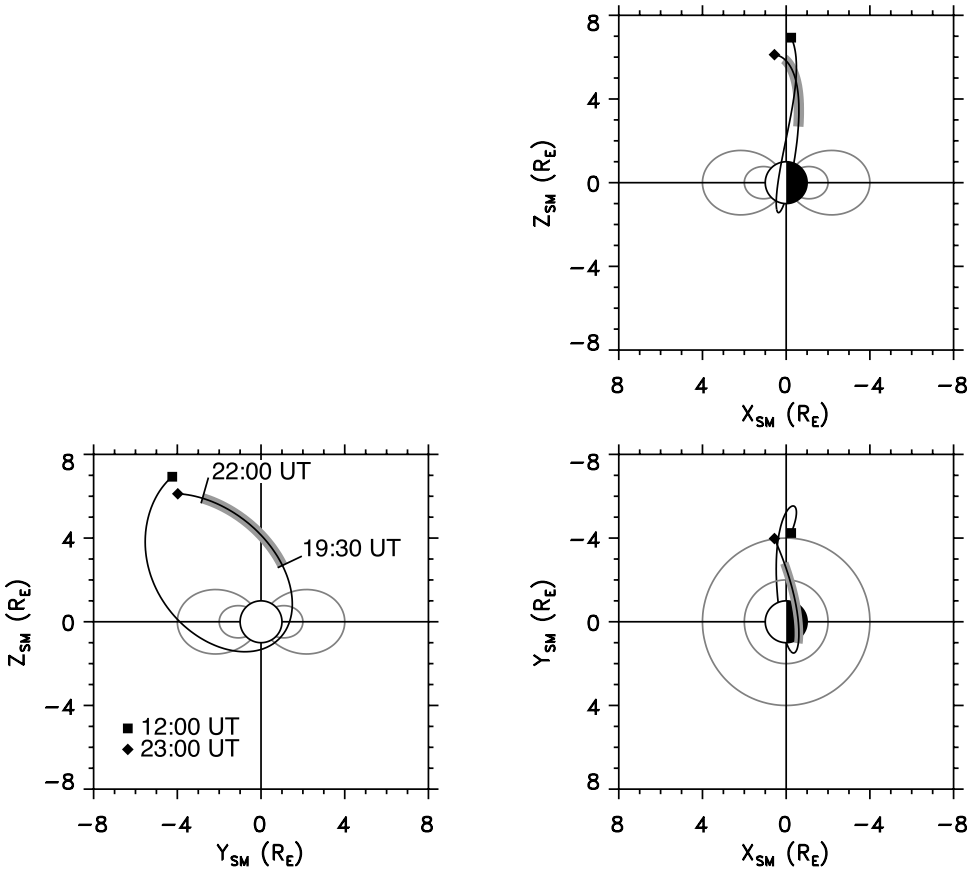

Figure 1. IMAGE orbit from 1200 to 2300 UT on 28 June 2000 highlighting in gray the period of observation from 1930 to 2200 UT. Dipole field lines of value L = 2 and = 4 have been plotted for reference.

and 0100 MLT appear to bifurcate and extend to $L \sim 2.5$ and beyond.

[10] A "residue" image [*Larson et al.*, 1986] is presented in Figure 3b that further illustrates the presence of these radial structures in the EUV data. The residue image is constructed by first rotating the original image by 8° counterclockwise about Earth center. The rotated image is then subtracted from the original image producing the linearly scaled residue image presented. The residue image shows a minimum in the crux of the 0200 MLT bifurcation while enhancing the bifurcated structure itself; indicates a weak minimum at the crux of the 0000 MLT bifurcation with enhancement of the bifurcation; and results in the entire structure of the 2200 MLT bifurcation being displayed as a minimum while the crux region is enhanced. Note that the minimum/enhancement character of each structure reverses when the residue image is produced by an 8° clockwise rotation of the original image. The residue image also indicates the presence of additional radial structures at 0500, 0700, and 0800 MLT. Tracing the δCount = 0 contour of Figure 3b "by eye" produces the plasmaspheric feature "cartoon" of Figure 3c that delineates the feature boundary (red) and the presence of the bifurcated, radial structures in question.

3.2. Existence Check

[11] These observed low L shell features appear in the nightside plasmasphere and progress toward dawn through Earth's shadow, a region that is typically dominated by a lack of emission [e.g., *Sandel et al.*, 2001, Figure 4; *Goldstein et al.*, 2003, Figure 3], while remaining visible. To illustrate the uniqueness of the event under study, Figure 4a presents one of the earliest EUV images of the plasmasphere recorded at 0555 UT on 24 May 2000 (day 145) in comparison to the image of Figure 3a. In the 24 May 2000 image a clear, distinct plasmapause is observed in addition to a well-defined shadow behind the Earth; features not readily evident in images from 28 June 2000. Therefore it is apparent that EUV observes features in the Earth's shadow, a region of the plasmasphere not normally visible.

[12] In order to demonstrate that the features observed progressing through and within Earth's shadow on 28 June 2000 (Figure 3b) are indeed plasmaspheric in nature, we present an explanation of the viewing geometry for this date. Figure 5 presents this event's geometry using dipole field lines from $1.5 \leq L \leq 2.5$ in Geocentric Solar Ecliptic (GSE) coordinates with Figure 5a displaying their projection in the XZ plane, while Figure 5b displays their projection in the XY plane. Note that those portions of individual field lines lying within the Earth shadow have been dashed to add perspective. Since the event in question occurs ~7 days post-summer solstice, Earth's geomagnetic field is tipped to its maximum extent toward the Sun at this time, as illustrated in the GSE XZ plane of Figure 5a. As a result, these low-L plasmaspheric field lines are tilted sufficiently above Earth's shadow to allow illumination of

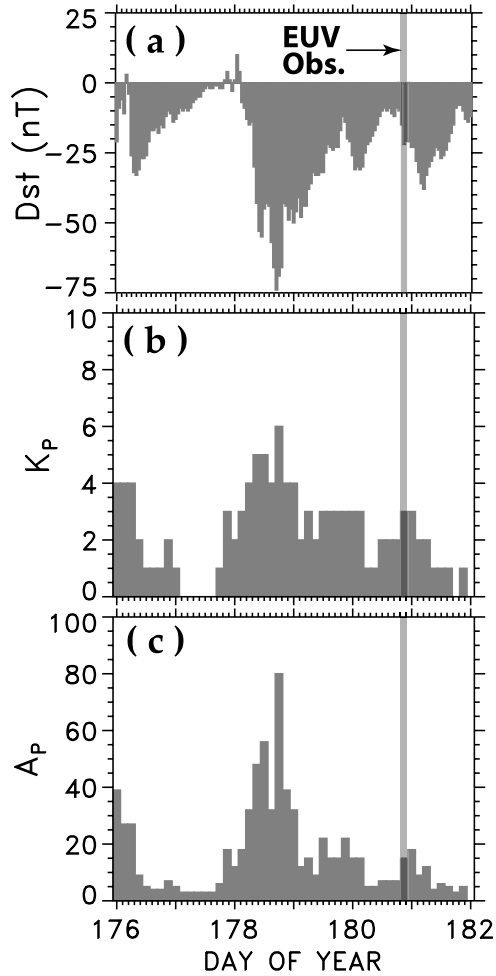

Figure 2. Geomagnetic conditions, bracketing the presented EUV observations, for days 176–182 (24–30 June) 2000 as characterized by the (a) *Dst*, (b) *Kp*, and (c) *Ap* indices.

these flux tubes by solar UV and subsequent imaging by EUV.

[13] While EUV imaging of an isolated flux tube has been reported [*Sandel et al.*, 2001], further examination of the geometry of the dipole magnetic field in GSE coordinates, particularly the projection in the *XY* plane presented in Figure 5b, demonstrates that neither arguments of off-pole viewing or twisting of an individual magnetic flux tube can be used to explain the observed bifurcated features. First, in order to have a field line geometry that appears split, the viewing geometry would have to allow for the ability to view both the northern and southern hemispheric segments simultaneously, while the equatorial section is shadowed; an invalid condition for this event according to Figure 5a. Even if both hemispheric sections of a field line were visible, Figure 5b indicates that while the imaging of the field line would have a split appearance, each segment of the split feature would appear radially aligned back toward Earth; a condition not observed by EUV for this event. Additionally, such a coupled viewing and field line geometry would not account for the observation of the split occurring as the higher-*L* extension of a lower-*L* radial feature. Therefore from Figure 5b it is clear that off-pole viewing of the region

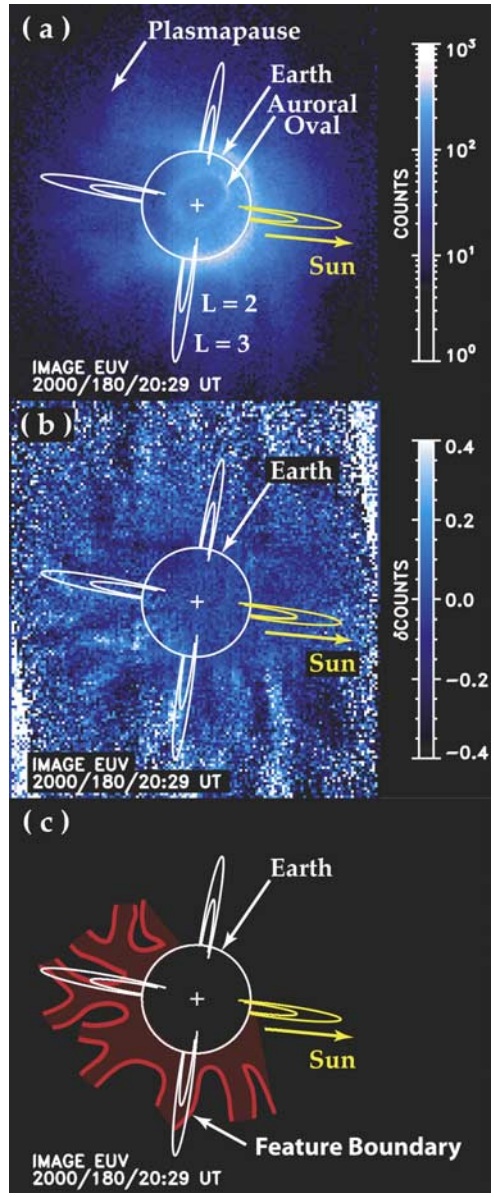

Figure 3. (a) He^+ plasmaspheric distribution taken by EUV at 2029 UT on 28 June 2000. The plasmapause is somewhat diffuse and displays bifurcated, radially structured enhancements in the nightside region. (b) Residue image of the 2029 UT data created by differencing the original image with one produced after an 8° counterclockwise rotation of the image about Earth center. The resultant residue highlights the presence of bifurcated, radial features at 2200, 0000, and 0200 MLT in addition to other radial features at 0500, 0700, and 0800 MLT. (c) Cartoon trace of the plasmapause (red) highlighting the presence of plasmaspheric features observed in residue image. For reference, the limb of the Earth is indicated with a white circle, and the dipole field lines for $L = 2$ and 3 at 0600, 1200, 1800, and 2400 MLT have been overlaid onto each plot with the 1200 MLT field lines in yellow to indicate the direction to the sun.

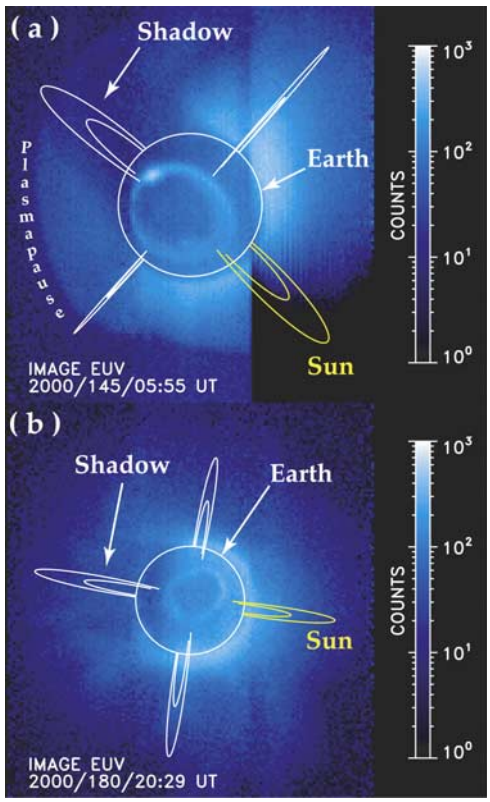

Figure 4. Comparison of EUV images recorded at (a) 0553 UT on 24 May (day 145) and (b) 28 June (day 180) 2000 highlighting the lack of a clear, distinct shadow region in the day 180 images due to the presence of bifurcated, radial He^+ enhancements. The Earth limb and $L = 2$ and 3 dipole field lines are overlaid for reference.

does not allow for a single field line, or flux tube, to appear split as observed in the EUV data. Furthermore, even if some mechanism existed that torsionally twisted a single field line (flux tube) in this region, the geometry of Figure 5a demonstrates that it would not be possible to view two distinct segments of such a field line simultaneously since only that portion above the limb shadow would receive solar illumination. In order to simultaneously view two distinct segments of a single twisted flux tube, that is have one segment lying above the limb shadow with another lying below the shadow, some mechanism would have to be present that would "stretch" or "pull" the lower segment of the flux tube below the lower extent of the limb shadow. Since there is no evidence from previous in situ magnetic field measurements of this type of twisting/stretching of flux tubes in the nightside plasmasphere, this scenario is highly unlikely. Consequently, the observed features cannot be attributed to either viewing geometry or deformation of single flux tubes and must, therefore, be the manifestations of another type of physical process.

3.3. Stability and Corotation Analysis

[14] EUV observes these bifurcated radial features from the onset of imaging for this orbit at 1933 UT until ~2221 UT. While EUV observations of the plasmasphere continue until 2307 UT, the orbit of IMAGE takes EUV beyond an ideal pole-viewing geometry (see Figure 1). Consequently, the line of sight of EUV becomes oblique/orthogonal to the radial features and, as such, results in a viewing geometry that is no longer conducive to observation of the features. It should also be noted that no indication of these features was present in EUV observations from the previous orbit (day 180; 0531–1240 UT). EUV data from the previous orbit is characterized at 0707 UT by a distinct plasmapause that contains a dual-lobed notch (J. L. Green et al., Association of kilometric continuum radiation with plasmaspheric structures, submitted to *Journal of Geophysical Research,* 2003). in the plasmapause extending from ~0230 to 0630 MLT that appears to be ε-shaped, a plasmaspheric drainage plume that appears to link to the 0630 MLT extent of the ε-shaped notch, and what appears to be the remnants of a narrow low-density channel that extends from

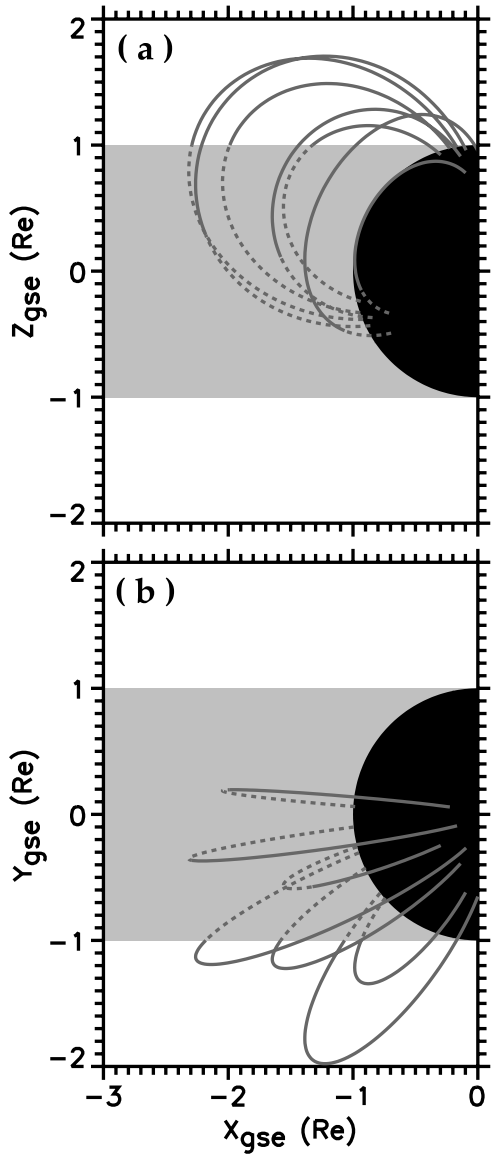

Figure 5. Configuration of the geomagnetic field with respect to Earth's shadow on 28 June 2000 presented in Geocentric Solar Ecliptic (GSE) coordinates for (a) the *XZ* plane and (b) the *XY* plane. Portions of each respective field line shadowed by the Earth have been dashed.

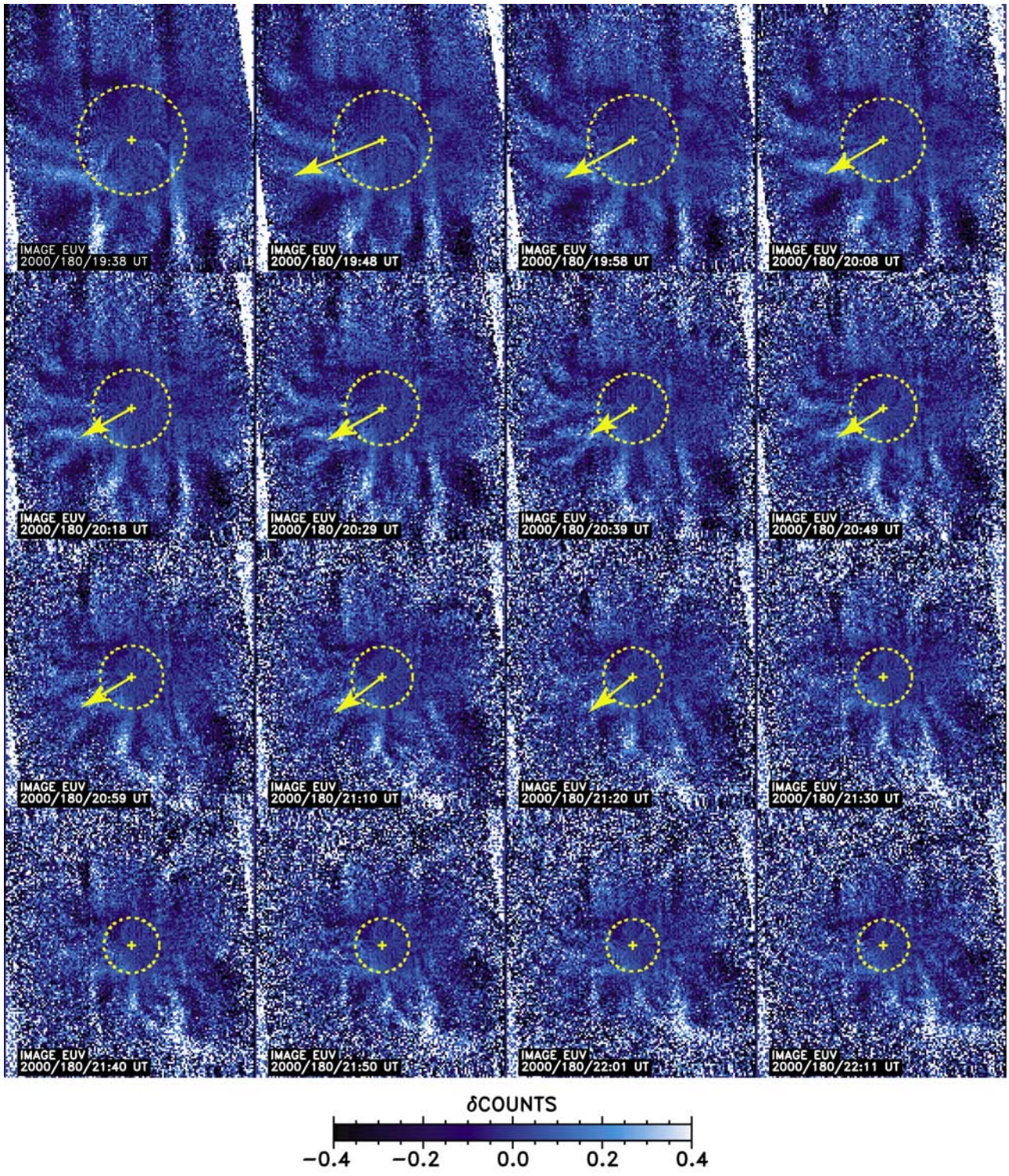

Figure 6. Time series of linearly scaled residue EUV images of the He^+ plasmaspheric distribution for 28 June 2000 showing the presence of bifurcated radial structures throughout the period of observation. In those residue images where the crux of the leading bifurcated feature is visible, a yellow arrow has been added, referenced to Earth's center, to indicate the location of the crux.

~1800 to 2200 UT. By the end of EUV operations during this orbit at ~1222 UT, the position of the ε-shaped notch appears to have corotated to about midnight. Under the assumptions of stability and corotation, the ε-shaped notch would have been observed in the dawn to postdawn sector in 1933 UT EUV data. However, neither the ε-shaped notch, the drainage plume, nor the low-density channel appears to have survived to the observations reported here. Therefore it is unlikely that

the bifurcated radial features observed by EUV from 1930 to 2200 UT evolved from the ε-shaped notch observed during the previous orbit since evolution from this previous structure would have required the notch to have either stagnated against corotation near midnight for an excess of 7 hours or experienced supercorotation. There is, however, no evidence in any of the EUV data from 28 June 2000 to support the existence of either condition. Therefore the formation of the features observed in Figure 3 appears to have occurred during the period between EUV turn off at 1230 UT of the previous orbit and EUV turn on at 1933 UT herein. Additionally, from the EUV instrument perspective, the bifurcated radial density structures appear to disappear toward the end of this observing period; however, the changing viewing perspective is sufficient for this to occur without any change in the density distribution.

[15] EUV observations demonstrate that the features are stable during the 2.5 hours of optimal viewing. Figure 6 presents a time series of linearly scaled residue images of EUV data acquired from 1938 to 2211 UT on 28 June 2000. In those residue images of Figure 6 where the crux of the leading bifurcated feature is visible, a yellow arrow has been added to indicate the location of the crux. Under the assumption that the observed features are constrained by dipole field lines and that the greatest contribution to integrated column intensity is supplied by plasma constrained to the minimum L shell intercepted by an EUV line-of-sight vector, the position (L-MLT) of any given feature can be mapped into the equatorial plane of the Solar Magnetic (SM) coordinate system [*Roelof and Skinner*, 2000]. Figure 7a shows a 40-min sequence of the mapped L-MLT position of the bifurcation feature previously shown at ~0100 MLT in Figures 3a and 3b. The data show that the feature advances steadily through the postmidnight sector toward dawn during this period. Tracking the crux of the feature, Figure 7b, reveals that the feature progresses linearly in time. Applying a linear least squares fit to the position of the bifurcation crux as a function of time (minutes past 2000 UT) yields the result

$$\mathrm{MLT} = 0.35 + 0.011 T_{\mathrm{minutes}}. \quad (1)$$

Similar results are obtained from an analysis of the proceeding feature. For comparison, the dashed line in Figure 7b corresponds to motion due to simple corotation. Since corotation proceeds at a rate of 1 hour of MLT per hour ($\omega = 1.\bar{6} \times 10^{-2}$ MLT min^{-1}), equation (1) indicates that the observed features progress toward dawn at 67% of corotation. This is an extraordinary result in light of the prevailing expectation that plasma at these small L shell values should strictly corotate with the Earth.

4. Discussion

4.1. E × B Convection: Simple Model

[16] In the previous section we have demonstrated that EUV observes bifurcated radial features in the nightside plasmasphere He^+ distribution. These features occur during a period of low geomagnetic activity, persist throughout the 2.5 hours of optimal viewing, and progress eastward at only 67% of the corotation rate. At first glance, the pattern of bifurcated radial enhancements suggests the presence of a $\mathbf{E} \times \mathbf{B}$ convective motion in the nightside plasmasphere driven by the radial electric field of an azimuthal standing wave. To test this hypothesis of plasmaspheric structure formation, we have constructed a simple two-dimensional particle simulation to test the influence of this type of localized convection in the inner magnetosphere. The simulation is populated by 10^4 ions uniformly distributed in a grid bounded by $-4 \le X_{\mathrm{SM}}\ (R_E) \le 4$ by $-4 \le Y_{\mathrm{SM}}\ (R_E) \le 4$ in the SM equatorial plane. The ions are then exposed to a radial electric field standing wave pattern centered at L = 1.8 and 2.5, based upon the EUV observations, in the presence of a dipole magnetic field. Neither corotation nor magnetospheric convection is included in the simulation. The electric field of each standing wave pattern (i = 1, 2) is assumed to be Gaussian in L and represented by the form

$$E_i = 2E_o \exp\left[-\frac{(L - L_{o,i})^2}{\sigma_i^2}\right] \sin(k_i\varphi)\cos(\omega t), \quad (2)$$

where E_o is the baseline electric field amplitude, $L_{o,i}$ is the L shell of the electric field maximum, σ_i is the L shell width (e^{-1}) of the electric field strength centered at $L_{o,i}$, $k_i = 2\pi/\lambda_i$ is the azimuthal wave number of each pattern, and $\omega = 2\pi/\Gamma$ is the angular frequency of each standing wave term. In order to simulate the features observed on 28 June 2000, the above parameters have taken the values E_o = 50 mV m^{-1} and $\sigma_1 = \sigma_2 = \Delta L = 0.5$, while $L_{o,1}$ = 1.8 and $L_{o,2}$ = 2.5, respectively. The standing wave pattern is assumed to possess wavelengths of 1.0 and 0.5 hours MLT at L = 1.8 and 2.5, respectively, and Γ = 33 min. The initial electric field amplitude distribution of the simulation is presented in Figure 8. Once the baseline electric field amplitude (E_o) and period (Γ) of the standing wave pattern are established, the focus of the simulation is restricted to plasma in the range $1.1 \le L \le 2.5$ and the simulation is allowed to proceed through N cycles or time steps of the standing wave pattern. For each time step of the simulation, the convection velocity of each test particle is calculated by determining the equatorial electric and dipole magnetic field amplitudes for the particle's location. This convection velocity is then used to calculate the equatorial displacement (dx, dy) of each test particle for that time step and a new particle location is calculated.

[17] The physics defining the particle dynamics of the simulation are summarized in the one-dimensional illustration of Figure 9. The presence of a standing wave electric field embedded in the dipolar geomagnetic field leads to the generation of a $\mathbf{E} \times \mathbf{B}$ convection velocity. The alternating polarity nature of the standing wave packets results in the generation of a sequence of alternating convection velocities. To understand the cumulative effect of this sequence of alternating convection velocities, consider the center pair of oppositely polarized wave packets in Figure 9. Here, the convection velocities of the pair point toward one another and toward the amplitude node or minimum centered between the packets. This results in the drift or "sweeping" of plasma concurrent with the wave packets away from the outer boundaries of the wave packets and toward the node. The cumulative consequence of the sequence of alternating polarity wave packets is the "sweeping" accumulation of

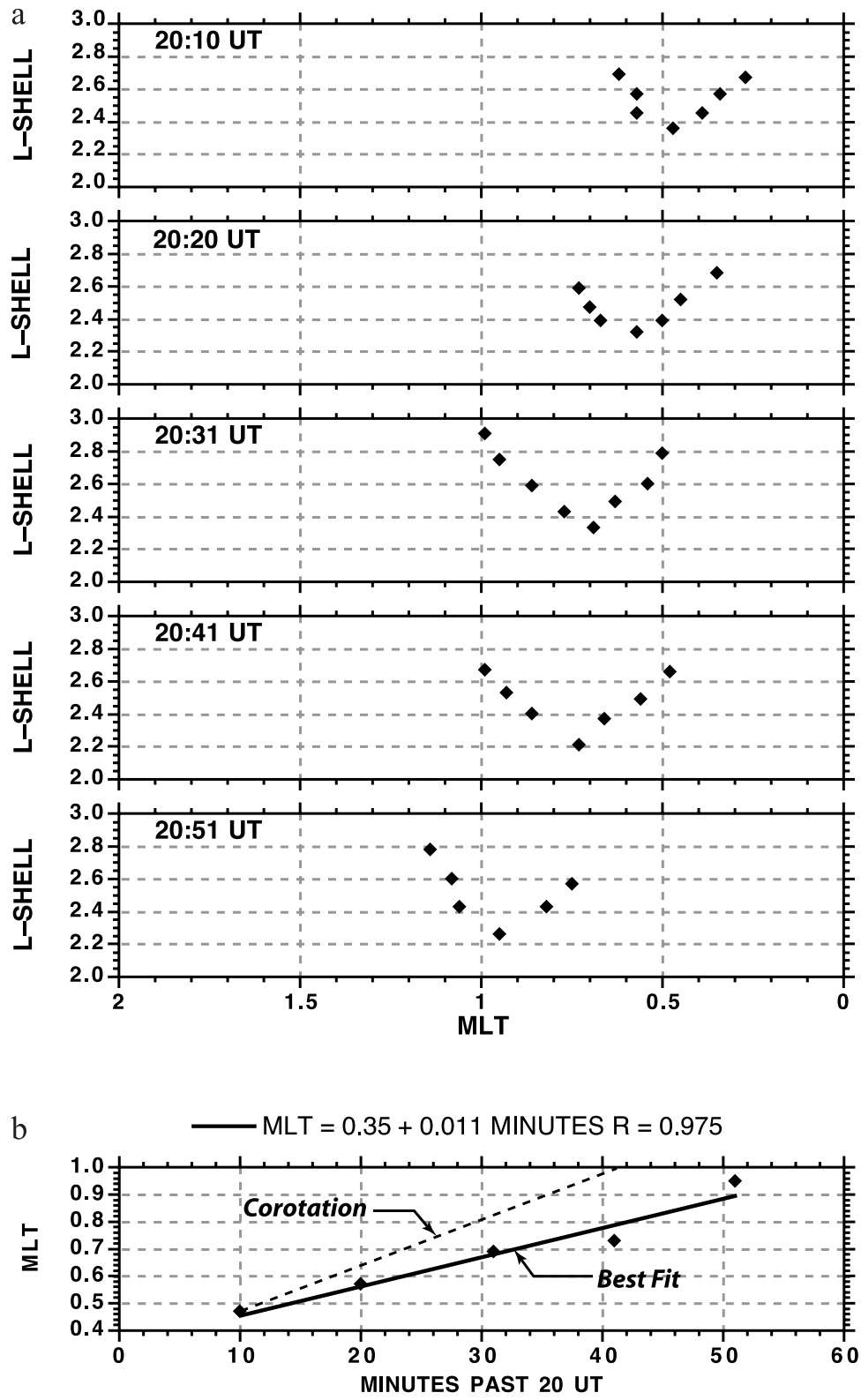

Figure 7. (a) Time sequence of Solar Magnetic *L*-MLT mapped coordinates of the premidnight bifurcation specified as the 2200 MLT bifurcation feature of Figure 3a. (b) Plot of the crux L-MLT location as a function of minutes past 2000 UT.

plasma into alternating wave nodes while plasma is evacuated from the successive neighboring nodes. The extent of this "sweeping" effect is illustrated in Figure 10, which presents a comparison of the EUV observation at 2029 UT (Figure 10a) with results from the convective simulation (Figure 10b). It must be noted that the degree of "sweeping" produced by the simulation is dependent on the amplitude and period of the standing wave; i.e., a weaker

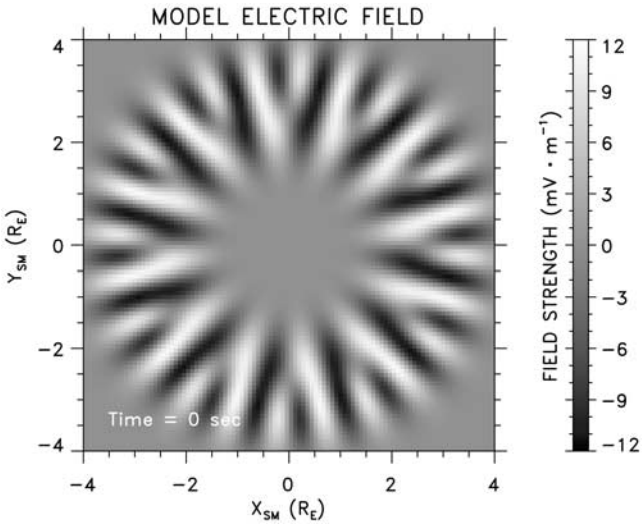

Figure 8. Initial distribution of electric field amplitudes for the two-dimensional test particle simulation of enhancements of plasmaspheric He^+ observed by IMAGE EUV on 28 June 2000. The electric field distribution is the result of the superposition of two resonances defined by equation (2), where E_o = 50 mV m^{-1}, $L_{o,1}$ = 1.8 and $L_{o,2}$ = 2.5, respectively, $\sigma_1 = \sigma_2 = L = 0.5$, the assumed wavelengths of the resonances are 1.0 and 0.5 hour MLT for L = 1.8 and 2.5, respectively, and Γ = 33 min.

amplitude coupled to a longer period results in the same distribution of test particles.

[18] It should be noted that this simple model is intended solely to suggest a mechanism that may be capable of creating the bifurcated radial density observed by IMAGE EUV on 28 June 2000. It must be pointed out that the use of a baseline electric field amplitude of 50 mV m^{-1} in order to replicate the observed plasmaspheric pattern is worrisome at best since the authors are not aware of any in situ observations of fields of this amplitude. Also, it must be recognized that the oscillatory nature of equation (2) will result in the structure shown in Figure 10b only at $\frac{1}{4}\Gamma$, and that by $\frac{1}{2}\Gamma$ the features will be washed out due to the changing polarity of the standing wave packet electric field. Consequently, if the features observed by EUV were the product of an azimuthal standing wave phenomenon in the inner magnetosphere, this phenomenon must have been strongly dampened. In addition, this simple model makes no effort to explain the observed lag in the motion of the observed features with respect to corotation. A more robust analysis of this event is left for future study.

[19] While the simple two-dimensional simulation presented here generally reproduces the features observed by EUV on 28 June 2000, the result is further tempered by the existence of two additional disparities/issues:

[20] 1. The long-wave periods required by the simulation to produce the bifurcated radial enhancements suggests that the ULF wavelength is larger than the physical dimensions of the inner magnetosphere [*Lessard et al.*, 2003], thereby (apparently) excluding field-aligned resonance and cavity mode oscillations as possible formation mechanisms for the observed features.

[21] 2. The conspicuous absence of EUV observations of dayside radial enhancements suggests that the azimuthal extent of these postulated waves is confined to a longitudinal window, ~6 hours wide in MLT roughly centered on midnight, as the result of either unidentified azimuthal

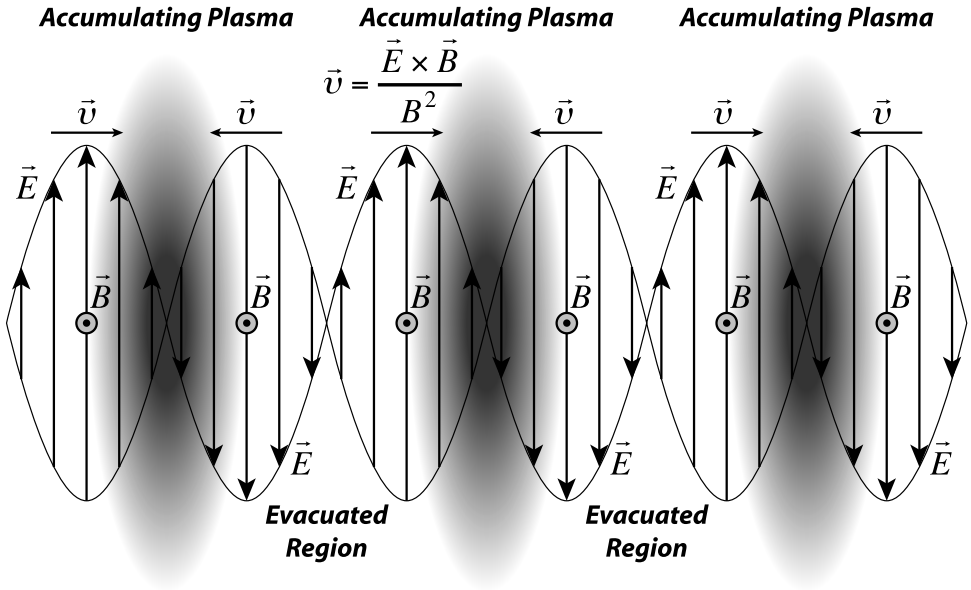

Figure 9. One-dimensional illustration of the physics involved in the simple two-dimensional test particle simulation of the 28 June 2000 event. The electric field of the standing wave pattern embedded in the dipole geomagnetic field leads to the generation of an **E** × **B** convection velocity. For a given pair of oppositely polarized wave packets, the combined effect of the convection velocity of the wave packets results in a drift of plasma toward the amplitude node or minimum located between the packets. This produces a "sweeping" of plasma into their common node and away from the neighboring successive nodes. The cumulative effect is the production of a structure of alternating plasma enhancements and voids.

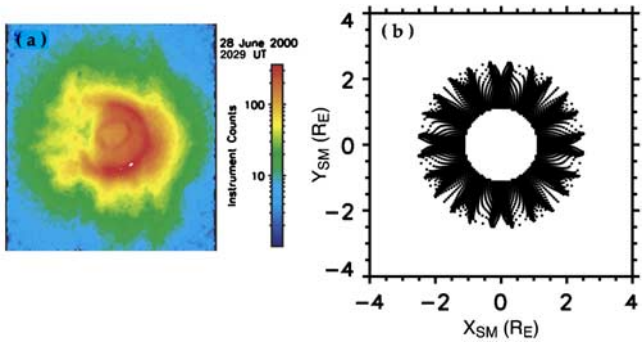

Figure 10. Comparison of (a) logarithmically scaled EUV image taken at 2029 UT on 28 June 2000 with (b) the result of a simple two-dimensional electrostatic test particle simulation of convection.

boundaries or low frequency wave focusing in the nightside inner magnetosphere.

[22] Rectification of these issues may be possible through the analysis of concurrent ground-based magnetometer and solar wind observations.

4.2. Initial Ground-Based Magnetometer Analysis

[23] Identification and quantification of any plasmaspheric or inner magnetospheric waves associated with the EUV-observed bifurcated radial He^+ distribution enhancements may be facilitated by analysis of dayside and nightside ground-based magnetometer data. Preliminary analysis of data from the International Monitor for Auroral Geomagnetic Effects (IMAGE) ground-based magnetometer network [*Lühr et al.*, 1998], covering L shell values from 3 to 15, has been completed with striking results. Figure 11 presents the geographical orientation, with relation to the terminator, of the IMAGE network at 2020 UT on 28 June 2000. The location of the Abisko, Sweden station, whose data is presented in the discussion that follows, has been indicated with a cross. It is evident from this plot that the IMAGE network was located on the nightside near the 2200 MLT radial feature observed by EUV. Consequently, analysis of the IMAGE magnetometer data during this period should serve to quantify the presence of ULF waves concurrent with the EUV observations.

[24] An example of the analysis of IMAGE magnetometer data is shown in Figure 12 using data from the Abisko, Sweden (ABK) station (L = 5.719). Figure 12a presents a frequency-time spectrogram of wave power for the X component of the ambient magnetic field from 1500 to 2359 UT on 28 June 2000. The intensity of the spectrum begins to increase at ~1900 UT in the 0.1–5.1 mHz frequency range, forming several discrete frequency components. Note that the rise in wave power occurs just prior to EUV observation of the bifurcated radial He^+ enhancements. The activity continues until ~2215 UT at which point the components above 3 mHz abruptly cease and the power of the lower frequency components recedes. The time period of enhanced wave power in the X component of the magnetic field brackets that of the EUV observations. The power spectrum from 2047:30 UT is presented in Figure 12b and displays the presence of six distinct narrow frequency components (0.68, 1.07, 1.76, 2.54, 3.52, and 4.20 mHz) associated with this event. While there is evidence of harmonics ($f_5 = 2f_3$) and coupled frequencies (i.e., $f_3 = f_1 + f_2$), identification of three-wave nonlinear processes is left for a future application of bispectral analysis.

[25] While the L shell location of the Abisko station is higher than that of the plasmaspheric features observed by EUV, Figure 8 suggests that the presence of a ULF standing wave pattern centered at $L_o = 2.5$ and with $\sigma = 0.5$ is capable of influencing plasma at higher L shells perhaps extending to Abisko station ($L > 4$). Therefore it is possible that the features observed in the Abisko wave power spectrogram are representative of the phenomenon responsible for producing the bifurcated radial plasma enhancements observed by EUV. Of course a complete determination of the radial and longitudinal extent of the ULF waves detected by Abisko will require a comprehensive analysis of all available ground-based magnetometer data with respect to L shell and MLT.

[26] As with the results from the simple two-dimensional simulation discussed above, the detection of discrete spectral features extending down to 0.68 mHz (Γ = 24.5 min) in the IMAGE ground-based magnetometer data leads to wavelength estimates greater than that of any previously reported field line or magnetospheric cavity resonance. Therefore it is unlikely that any such internal mechanism is responsible for both the EUV and ground magnetometer

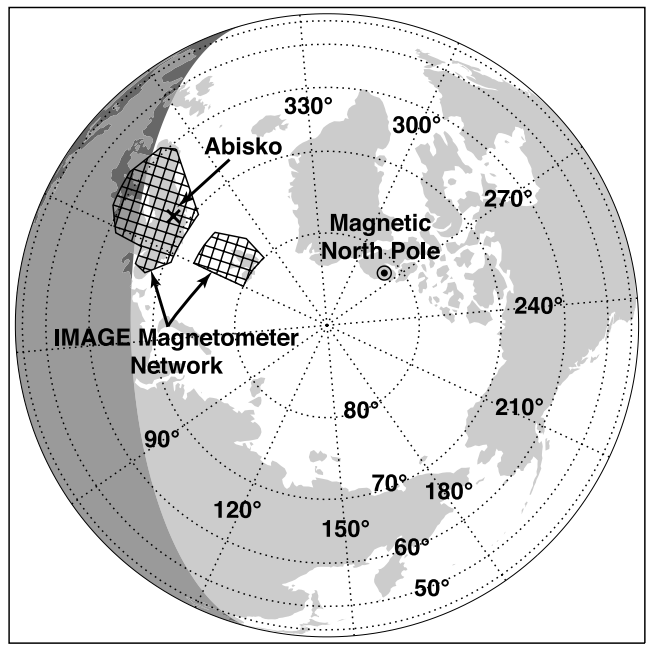

Figure 11. Geographical orientation of the northern hemisphere at 2020 UT on 28 June 2000 in the midst of the EUV-observed bifurcated radial He^+ enhancement event. The location of the geomagnetic North Pole has been indicated. The geographical region monitored by the IMAGE magnetometer network has been indicated by cross hatching and the location of the Abisko, Sweden (ABK), station is labeled with a cross.

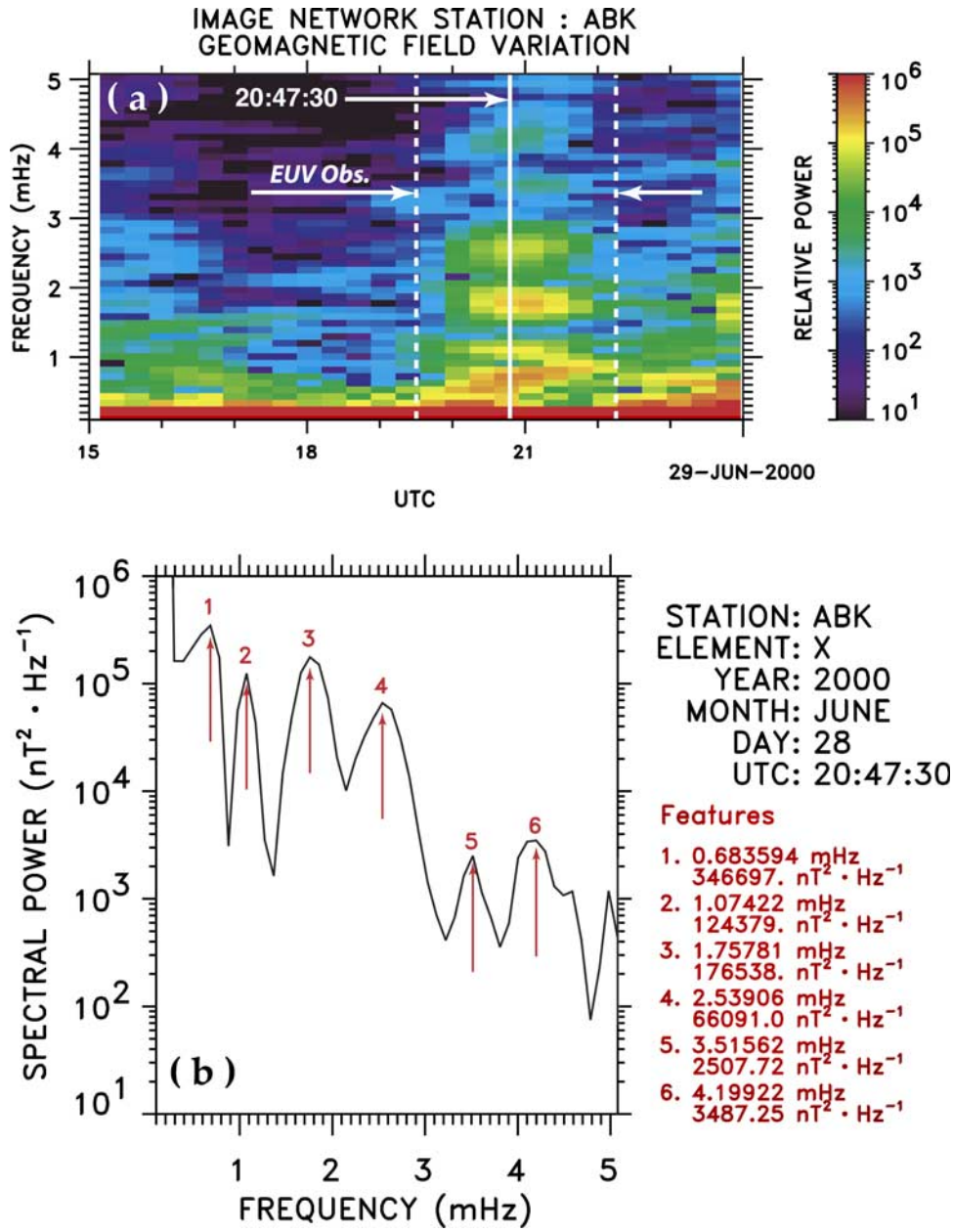

Figure 12. (a) Frequency-time spectrogram of wave power for the X component of geomagnetic field measured at Abisko (ABK) between 1500 and 2359 UT on 28 June 2000. The spectrogram indicates an increase in wave power at ~1900 UT just prior to EUV turn on and detection of the bifurcated radial enhancements in the plasmaspheric He+ distribution in the nightside plasmapause. The wave power then recedes at ~2215 UT, approximately the time EUV is no longer to resolve the plasmaspheric features. (b) Power spectrum at 2047:30 UT illustrating that the enhancement in wave power at 1900 UT coalesces to six distinct spectral components from 0.68 to 4.2 mHz.

observations. As a consequence, it is worthwhile to look for an external, nonresonant origin for what appears to be a standing wave feature in the EUV observations.

4.3. Preliminary Solar Wind Data Analysis

[27] Solar wind thermal plasma data acquired on 28 June 2000 by the Solar Wind Electron Proton Alpha Monitor (SWEPAM) [*McComas et al.*, 1998] aboard the Advanced Composition Explorer (ACE) satellite offers clues to an external mechanism. On this date, ACE was located ~242 R_E upstream in the solar wind virtually on the X axis in GSE coordinates. Very preliminary spectral analysis of SWEPAM bulk velocity data indicates the onset of several narrow frequency features, possibly extending down into the sub-mHz regime, at ~1700 UT. Accounting for propagation at ~470 km s^{-1} these features arrived at the bow shock and magnetopause regions of near-Earth space in excess of ~54 min later, or at ~1800 UT; an hour in advance of the EUV observations. These narrow-frequency features in the bulk solar wind velocity evolve over the next

Table 1. Summary of EUV-Observed Radial He^+ Enhancements For Year 2001[a]

Date	Time (UT)	*Dst* (Range)	*Kp*
2001/02/18	1637–0027	0 ↔ 11	5−
10 March 2001	0806–1404	−6 ↔ −1	2+
14 March 2001	1136–1856	−2 ↔ 1	2+
18 March 2001	1546–2214	−7 ↔ 2	2+
19 March 2001	0552–1049	−105 ↔ −12	2
26 March 2001	0652–1412	−13 ↔ −9	1− ↔ 2+
17 April 2001	2009–0339	−17 ↔ 6	2+ ↔ 3+
6 May 2001	0501–1342	5 ↔ 8	0 ↔ 2+
21 May 2001	1529–2229	8 ↔ 12	1− ↔ 7−
22 May 2001	0446–1349	18 ↔ 28	1+ ↔ 2
31 May 2001	0245–0945	0 ↔ 4	0
6 June 2001	0036–0906	13 ↔ 20	1 ↔ 2+
11 June 2001	2256–0829	−3 ↔ 5	2
12 June 2001	1405–2206	−5 ↔ 6	1+
16 June 2001	0233–1237	12 ↔ 19	2− ↔ 1+
27 June 2001	2259–0912	8 ↔ 13	0
29 June 2001	0405–1329	18 ↔ 19	0
2 July 2001	1746–0116	−4 ↔ 6	1−
19 July 2001	2259–0741	−8 ↔ −3	1− ↔ 2+
12 Aug. 2001	0243–1044	−4 ↔ −9	3− ↔ 3+

[a]Date of the event, the time period of observation, the range of *Dst* (format min ↔ max), and *Kp* that occurred during the period of event observation.

5+ hours developing harmonic and coupled-wave behavior similar to that displayed in the Abisko ground magnetometer data. Thus we speculate that the concurrent standing wave pattern in helium ions observed by EUV and the narrow-frequency features detected by the IMAGE ground-based magnetometer network may be the result of the transmission of solar wind pressure pulses into the inner magnetosphere.

[28] A full discussion of ground-based magnetometer and solar wind data analysis and resulting implications for source mechanism identification will be presented in a future paper.

5. Conclusions

[29] We have presented EUV observations of bifurcated radial enhancements in the He^+ distribution from 1938 to 2211 UT on 28 June 2000 in the nightside plasmasphere during a period of low geomagnetic activity. The initial impression of the bifurcated radial enhancements in EUV images is that of a standing wave pattern "frozen" into the nightside plasmasphere. Formation of these features has been replicated using a two-dimensional simulation of an azimuthal standing wave pattern (at L = 1.8 and 2.5) possessing Gaussian electric fields with $\Delta L = 0.5\ e^{-1}$ radial width. While the baseline electric field amplitude (50 mV m^{-1}) appears unphysical and the period (Γ = 33 min) of the simulated standing wave implies wavelengths in excess of the physical dimensions of the inter-magnetospheric cavity, preliminary analysis of IMAGE magnetometer network data indicates the presence of discrete spectral components, coincident with the EUV observations, with periods of 10's of minutes (f = 0.68 mHz ↔ Γ = 24.5 min). Since the simulated and observed wave periods lead to wavelength estimates greater than that previously reported for field line or magnetospheric cavity resonance, we speculate that the bifurcated radial enhancements in the nightside plasmaspheric He^+ distribution may result from a solar wind driven standing wave pattern in the inner magnetosphere. An in-depth analysis of available solar wind data proximate to this event is planned and the results of this effort will be published sometime in the future.

[30] While the bifurcated radial enhancements of He^+ distribution in the plasmasphere observed on 28 June 2000 are the most dramatic example of plasmaspheric dynamics observed to date, it is not the only example of observed radial enhancements. Table 1 presents an overview of 21 EUV-observed plasmaspheric radial enhancement events discovered in a survey of EUV data for 2001. The table presents the date of each event, the period of observation in Universal Time (UT), range of *Dst* (format min ↔ max), and range of *Kp* that occurred over the period of observation. Review of *Dst* and *Kp* indices associated with these events indicates that radial He^+ enhancements occur during periods of relative quiet. Only one radial enhancement event (2001/03/19) is associated with a moderate geomagnetic storm in excess of −100 nT and only one event (2001/04/17) is associated with a *Kp* index above 3. From the simple particle simulation presented here, the structure of these other events may also be attributed to an azimuthal electric field standing wave pattern. Clearly, this class of phenomena offers new insight into the dynamics of the plasmasphere and inner magnetosphere.

[31] **Acknowledgments.** The authors wish to thank B. R Sandel, W. T. Forrester, and R. A. King for their assistance in the processing and analysis of EUV data. The authors also wish to thank the Finnish Meteorological Institute as well as the institutes maintaining the IMAGE magnetometer array.

[32] Arthur Richmond thanks the reviewers for their assistance in evaluating this paper.

References

Brice, N. M. (1967), Bulk motion of the magnetosphere, *J. Geophys. Res.*, *72*, 5193.

Burch, J. L., et al. (2001), Views of the Earth's magnetosphere with the IMAGE satellite, *Science*, *291*, 619.

Carpenter, D. L. (1963), Whistler evidence of a 'knee' in the magnetospheric ionization density profile, *J. Geophys. Res.*, *68*, 1675.

Chakrabarti, S., F. Paresce, S. Bowyer, S. Chiu, and A. Aikin (1982), Plasmaspheric Helium ion distribution from satellite observations of He II 304 Å, *Geophys. Res. Lett.*, *9*, 151.

Comfort, R. H., I. T. Newberry, and C. R. Chappell (1988), Preliminary statistical survey of plasmaspheric ion properties from observations by DE 1/RIMS, in *Modeling Magnetospheric Plasma*, *Geophys. Monogr. Ser.*, vol. 44, edited by T. E. Moore and J. H. Waite Jr., p. 107, AGU, Washington, D. C.

Craven, P. D., D. L. Gallagher, and R. H. Comfort (1997), Relative concentration of He^+ in the inner magnetosphere as observed by DE 1 retarding ion mass spectrometer, *J. Geophys. Res.*, *102*, 2279.

Goldstein, J., M. Spasojevi, P. H. Reiff, B. R. Sandel, W. T. Forrester, D. L. Gallagher, and B. W. Reinisch (2003), Identifying the plasmapause in IMAGE EUV data using IMAGE RPI in situ steep density gradients, *J. Geophys. Res.*, *108*(A4), 1147, doi:10.1029/2002JA009475.

Gringauz, K. I. (1963), The structure of the ionized gas envelope of the Earth from direct measurements in the USSR of local charged particle concentrations, *Planet. Space Sci.*, *11*, 281.

Horwitz, J. L., R. H. Comfort, and C. R. Chappell (1990), A statistical characterization of plasmasphere density structure and boundary locations, *J. Geophys. Res.*, *95*, 7937.

Kivelson, M. G., and D. J. Southwood (1985), Resonant ULF waves: A new interpretation, *Geophys. Res. Lett.*, *12*, 49.

Larson, S., Z. Sekanina, D. Levy, S. Tapia, and M. Senay (1986), Comet Halley near-nucleus phenomena in 1986, in *20th ESLAB Symposium on the Exploration of Halley's Comet: Proceedings of the International Symposium*, vol. 2, edited by B. Battrick, E. J. Rolfe, and R. Reinhard, *Eur. Space Agency Spec. Publ.*, *ESA SP-50*, 145.

Lessard, M. R., J. Hanna, E. F. Donovan, and G. D. Reeves (2003), Evidence for a discrete spectrum of persistent magnetospheric fluctuations below 1 mHz, *J. Geophys. Res.*, *108*(A3), 1125, doi:10.1029/2002JA009311.

Lühr, H., A. Aylward, S. C. Buchert, A. Pajunpää, K. Pajunpää, T. Holmboe, and S. M. Zalewski (1998), Westward moving dynamic substorm features observed with the IMAGE magnetometer network and other ground-based instruments, *Ann. Geophys.*, *16*, 425.

McComas, D. J., S. J. Bame, P. Barker, W. C. Feldman, J. L. Phillips, and P. Riley (1998), Solar Wind Electron Proton Alpha Monitor (SWEPAM) for the Advanced Composition Explorer, *Space Sci. Rev.*, *86*, 563.

Meier, R. R., and C. S. Weller (1974), Extreme ultraviolet observations of the latitudinal variation of Helium, *J. Geophys. Res.*, *79*, 1575.

Meier, R. R., A. C. Nicholas, J. M. Picone, D. J. Melendez-Alvira, G. I. Ganguli, M. A. Reynolds, and E. C. Roelof (1998), Inversion of plasmaspheric EUV remote sensing data from the STP 72-1 satellite, *J. Geophys. Res.*, *103*, 17,505.

Moore, T. E., D. L. Gallagher, J. L. Horwitz, and R. H. Comfort (1987), MHD wave breaking in the outer plasmasphere, *Geophys. Res. Lett.*, *14*, 1007.

Nakamura, M., I. Yoshikawa, A. Yamazaki, K. Shiomi, Y. Takizawa, M. Hirahara, K. Yamashita, Y. Saito, and W. Miyake (2000), Terrestrial plasmasphere imaging by an extreme ultraviolet scanner on Planet-B, *Geophys. Res. Lett.*, *27*, 141.

Nishida, A. (1966), Formation of plasmapause, or magnetospheric plasma knee, by the combined action of magnetospheric convection and plasma escape from the tail, *J. Geophys. Res.*, *71*, 5669.

Roelof, E. C., and A. J. Skinner (2000), Extraction of ion distributions from magnetospheric ENA and EUV images, *Space Sci. Rev.*, *91*, 437.

Samson, J. C., B. G. Harrold, J. M. Rouhoniemi, R. A. Greenwald, and A. D. M. Walker (1992), Field line resonances associated with MHD waveguides in the magnetosphere, *Geophys. Res. Lett.*, *19*, 441.

Sandel, B. R., et al. (2000), The extreme ultraviolet imager investigation for the IMAGE mission, *Space Sci. Rev.*, *91*, 197.

Sandel, B. R., R. A. King, W. T. Forrester, D. L. Gallagher, A. L. Broadfoot, and C. C. Curtis (2001), Initial results from the IMAGE extreme ultraviolet imager, *Geophys. Res. Lett.*, *28*, 1439.

Sandel, B. R., J. Goldstein, D. L. Gallagher, and M. Spasojevic (2003), Extreme ultraviolet imager observations of the structure and dynamics of the plasmasphere, *Space Sci. Rev*, in press.

Swift, D. W., R. W. Smith, and S.-I. Akasofu (1989), Imaging the Earth's magnetosphere, *Planet. Space Sci.*, *37*, 379.

Weller, C. S., and R. R. Meier (1974), First satellite observations of the He^+ 304-Å radiation and its interpretation, *J. Geophys. Res.*, *79*, 1572.

M. L. Adrian, Center for Space Plasma and Aeronomic Research, University of Alabama in Huntsville, Huntsville, AL 35899, USA. (mark.l.adrian@msfc.nasa.gov)

L. A. Avanov and D. L. Gallagher, Science Directorate, SD50, NASA Marshall Space Flight Center, 320 Sparkman Drive, Huntsville, AL 35812, USA. (dennis.gallagher@msfc.nasa.gov)